INTERNATIONAL JOURNAL OF SCIENTIFIC INFORMATION
www.jsiinternational.com Research Article ISSN: 2583-8512

# Cationic Dyes Recovery from Water Using Nano adsorbents

**Shalfi Arya[1] and Yajvinder Saharan[1*]**

**[1]Department of Chemistry, School of Applied Sciences, Om Sterling Global University, Hisar**
**[*]Corresponding Author: Yajvinder Saharan**
**Email: yajvindersaharan5@gmail.com**

**Article Received on: 23/02/26; Revised on: 17/02/26; Approved for publication: 10/03/26**

**Keywords**
**Nanocomposites; Dyes; Thermodynamics; Adsorption; Isotherms**

***How to Cite this Article:***

**Arya S and Saharan Y. Cationic Dyes Recovery from Water Using Nano adsorbents. Int. J. Sci. Info. 2025; 3 (12): 11-38**

**ABSTRACT**

The present work is about the fabrication of ZnO and ZnO@PP nanocomposites and their application for dye sequestration from simulated water and has also been used for dye sequestration to evaluate the potential of nanocomposites. The SEM, FTIR and EDX techniques were employed for characterization of ZnO and ZnO@PP nanocomposites adsorbents. The dye experimental study was realized by batch adsorption study to explore the effect of various operating criterion on the elimination of dyes. The experimental data was subjected to thermodynamic; kinetic and isotherms models were investigated. Analysis of equilibrium data revealed a good fit with the Langmuir isotherm model, suggesting uniform monolayer adsorption on a homogeneous surface. This study suggested that due nanocomposites the removal of dyes could be possible and has greater potential for dye sequestration from effluent.

## 1. Introduction:

Most dyes are dangerous and non-biodegradable, and they are commonly found in industrial wastewater. When released into the environmental component, they can contaminate nearby soil and water system. With the course of time, these dyes can accumulate in natural ecosystems and enter the food chain and cause risks to both animal and human health. Therefore, it is important to remove or isolate these dyes from different environmental systems. (kataria and Garg., 2016).

At present, several different methods are used to treat dye-contaminated wastewater. These include physical, chemical and biological approaches. Physico-chemical techniques such as coagulation, membrane

separation, ion exchange, and adsorption are often effective and widely applied. However, many drawbacks are also associated with these, including high treatment costs and the generation of large amounts of sludge (Oteroa et al., 2009). The excessive sludge produced can create pollution of soil and natural water bodies. So, both developed and developing countries are actively seeking more efficient, affordable, and environmentally friendly treatment alternatives. The adsorption process was found to be a better, reliable and attractive alternatives, especially if the adsorbent is cost effective (Bulgariu et al., 2013). Nowadays, nanoadsorbents are found to be promising and innovative alternate to traditional adsorbents due to their smaller size, greater surface area, high regeneration efficiency, reuse potential, thermal stability and magnetic nature (Garg and Kataria, 2016; Ahlawat et al., 2019).

Photocatalysis has emerged as an effective and sustainable approach for the degradation of organic dyes in wastewater (Nazir,et al 2022A; Nazir,et al 2022B; Momeni,2015). This process involves chemical reactions initiated by ultraviolet or visible light when it irradiates the surface of a semiconductor material. Semiconductor-based heterogeneous photo catalysts such as $TiO_2$, ZnO, and ZnS have been extensively investigated for harnessing solar energy to address environmental pollution challenges (Liqiang, 2006). The photo catalytic activity of these materials is strongly dependent on their morphology and surface characteristics.

Among various semiconductors, zinc oxide is one of the most widely studied photo catalysts owing to its wide band gap of approximately 3.27 et at room temperature and high exciton binding energy. Zinc oxide nanoparticles possess several advantageous properties, including environmental compatibility, low cost, non-toxicity, and excellent chemical stability. These attributes have enabled their application in diverse fields such as cosmetics, electronics, and catalysis (Mahlambi, et al 2015; Ruszkiewicz et al 2017). Furthermore, the photocatalytic performance of ZnO can be significantly enhanced by surface modification or doping with noble and transition metals such as Au, Ag, and Cu (Guy, et al 2016; Rodrigues et al2020; Liu, et al 2015)

Zinc oxide nanoparticles can be synthesized through a variety of top-down and bottom-up techniques (Ul-Haq, et al 2017; Bandeira et al 2020; Mallakpour, et al 2012; Ma et al 2016). However, green synthesis methods using biological resources have attracted growing interest as eco-friendly and sustainable alternatives to conventional chemical routes (Mehmood, et al 2017). Potato, a widely cultivated tuber crop, is rich in starch, a natural polymer that is abundant, renewable, biodegradable, and inexpensive. Upon hydrolysis, starch yields amylose (a linear polymer) and amylopectin (a branched polymer). The interaction between these two components can form molecular frameworks that serve as effective templates for nanoparticle nucleation and growth (Mehmood, et al 2017).

Zinc oxide nanoparticles is also recognized as a sustainable photocatalyst, and its combination with Calcium oxide may result in improved photocatalytic efficiency (Mehmood, et al 2017). Recently Potato Starch-Assisted Synthesis of Zinc Oxide Nanoparticles and Calcium–ZnO Nanocomposites for Photocatalytic Removal of Methylene Blue and Rhodamine B has been reported (Sahu, 2023). Zinc oxide nanoparticles exhibit high surface area, which promotes greater adsorption of dye molecules on their surface. Hence, in the present section ZnO nanoparticles and ZnO loaded potato peel nanocomposites has been synthesized using potato peel as a natural

stabilizing and templating agent. The synthesized materials are evaluated through the degradation of two model dyes, Methylene Blue and Rhodamine B.

## 2. Experiments

### 2.1. Materials

The experimental chemicals and reagents were obtained from Sigma Aldrich Chemicals Private. Ltd., India, Himedia laboratory Private. Ltd., India, Mumbai and SD fine-Chemical Ltd, Mumbai. Dyes such as Methylene blue and Rhodamine B were procured from Himedia laboratory Pvt. Ltd., India. Activated carbon was procured from SD fine-chemical Ltd., India and all chemicals were of analytical grade. Deionised water (DW) was also obtained from laboratory to prepare stocks and experimental solutions.

### 2.2. Adsorbent fabrication process

#### 2.2.1. Synthesis of Zinc Oxide nanoparticles:

The Zinc oxide nanoparticles was synthesised by adding 3 g of zinc acetate dihydrate into deionized water under strong stirring at 65 °C on magnetic stirrer so that it is equally dispersed in solution. Subsequently, 5 g of Polyvinylpyrrolidone (PVP), capping agent, particularly for nanoparticle synthesis, helping to control size, shape, and prevent aggregation was added and well dissolved to the above solution maintaining same temperature. Further the solution was subjected to vacuum drying at 65 °C until we get solid substance, after that it was dried at 100 °C in oven and calcination at 600 °C for 60 minutes. Finally, we obtained nanocrystalline ZnO powder and grounded using pestle and motor.

#### 2.2.2 Synthesis of ZnO@PP nanocomposites

Potato peel waste was collected from home, cleaned many times, dried, crushed, sieved and finally powder and were kept 12 hours at 250 °C in a muffle furnace. A beaker with water ethanol ratio (1:2) were used; 3.0 g of synthesized ZnO nanoparticles were added to 12 g of PP in another beaker. The suspensions was first stirred for two hours and then kept in ultrasonic bath tub for 3 h under sonication. We obtained ZnO@PP nanocomposites after centrifugation, washing (twice with deionised water and ethanol) and calcination at 200°C. All adsorbents were stored in air tight bottle and were subjected to further characterization and experimentation.

### 2.3. Characterization of adsorbents

The crystallinity of manufactured ZnO, ZnO@PP nanocomposites were examined by XRD technique using Rigaku miniflex II Diffractometer. Chemical functional groups were identified using SHIMADIZU IR AFFINITY-1 FTIR spectrophotometer. Energy-dispersive X-ray spectroscopy technique was employed for elemental arrangement and morphology of the adsorbents was studied using Scanning electron microscope. UV-Vis spectrophotometer (LABINDIA UV 3000) used to determine the amount of dye removed from the water system.

**2.4. Dyes adsorptive experiments**

The experiments to evaluate efficiency of ZnO, ZnO@PP nanocomposites. The existence of functional groups on the surface of samples was recorded by Fourier transform infra-red technique (FTIR: Shimadzu IR AFFINITY-I, Japan and by making bits of samples mixed with KBr. For FTIR spectrum, pinch of sample (in powder form) was grinded well with KBr salt and bits were prepared from this mixture using disc pressure press. The bits were then analyzed under IR spectrophotometer.nanocomposites and adsorbent for eliminating dyes from aqueous system were conducted in batch mode under different process conditions. Two cationic dyes utilized in this work were Methylene blue and Rhodamine B and their stock solution were prepared (500mg/L) in one litre of deionized water by dissolving appropriate quantity of dye. Further dilution of the stock solution was done in proper manner to obtain the working solutions of different concentrations. For both the dyes, known concentration standard solution (10mg/L, 30mg/L .....100mg/L) were prepared and calibration curve was plotted between the known standard concentrations and absorbance using The removal of dyes and uptake capacity were determined following to equations given below (saini et al., 2019).

$$\text{Metal ion removal (\%)} = \frac{(C_o - C_e)}{C_o} \times 100 \quad (3)$$

$$\text{Adsorption capacity at equilibrium } (q_e) = \frac{(C_o - C_e)\, V}{m} \quad (4)$$

Where, Co (mg $L^{-1}$), and Ce (mg $L^{-1}$) are the initial and final metal ions concentration, m (g) denotes the adsorbent mass, V (L) denotes the volume of metal ions and qe (mg $g^{-1}$) denotes the uptake capacity of adsorbents at equilibrium.

**2.5. Reuse potential**

Reusability is important to evaluate the efficiency of adsorbent as eco-friendly and sustainable approach. , the reusability and regeneration efficiency of ZnO@PP nanoparticles were evaluated through four consecutive adsorption–desorption cycles, after completion of each adsorption experiment, the spent adsorbent was recovered from the aqueous phase by centrifugation. The separated material was subsequently washed repeatedly with ethanol followed by distilled water to remove residual dye molecules and then dried in an oven at 80 °C for several hours. The regenerated ZnO@PP nanoparticles were reused for subsequent adsorption cycles of cationic dyes.

**3. Results for Discussion:**

**.3.1 XRD characterization of ZnO@Potato Peel loaded nanoparticles**

Fig. 3.1 presents the XRD diffraction pattern of the synthesized ZnO@Potato Peel nanoparticles. The major diffraction peaks recorded at 2θ values of 31.21°, 34.81°, 37.14°, 47.15°, 57.0°, 64.87°, 66.54° and 69.17° correspond to the characteristic (100), (002), (101), (102), (109), (103), (198), (113), and (200) crystallographic planes of ZnO, respectively. These reflections confirm that the crystalline structure of the synthesized nanocomposite is consistent with the standard hexagonal wurtzite ZnO phase. In addition to these peaks, broad humps were observed at around 2θ = 26.8° and 43.9° for the Potato Peel component, which indicate the presence

of amorphous organic matter inherent to the biomass. The distinct and sharp reflections at 2θ ≈ 35° and 65° further validate the crystalline nature of the ZnO nanoparticles embedded within the composite. Moreover, the wide, less intense peaks appearing between 2θ = 20°–30° and 70°–90° reveal the amorphous characteristics of the Potato Peel matrix, suggesting partial structural changes after the synthesis process (Saini et al., 2017). These diffraction features are consistent with trends reported in earlier investigations on ZnO and biomass-based nanocomposites (Kataria and Garg, 2019), thereby confirming the successful formation of ZnO@Potato Peel nanoparticles with both crystalline and amorphous domains.

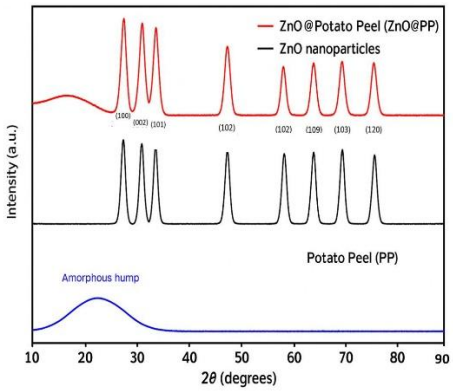


**Figure 3.1: XRD Characterization of Potato Peel, ZnO and ZnO Nanocomposites**

### 3. 2 FTIR spectra of ZnO@Potato peel Nanoparticles

Fig. 3.2 Fourier transform infrared (FTIR) spectroscopy was done to study the functional groups on the surface and potential binding sites present on the synthesized materials.

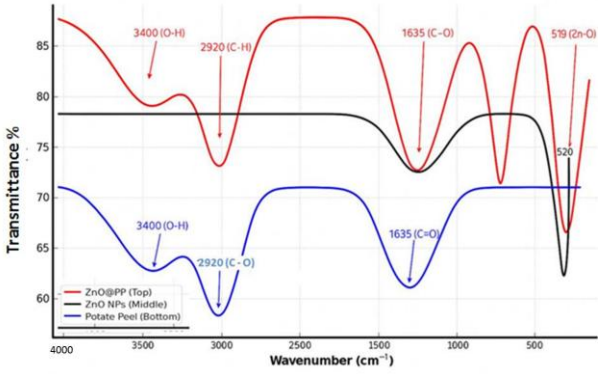


**Figure 3.2: FTIR spectra comparision of Potato Peel, ZnO and ZnO Nanocomposites**

The FTIR spectrum of ZnO @ Potato Peel (PP) displayed characteristic lower absorption bands at 3400 $cm^{-1}$ (O-H), 2920$cm^{-1}$ (C-H), 1635 $cm^{-1}$ (C-O), and 519 $cm^{-1}$ (Zn-O), stretching is observed, in Fig. 3.2 than ZnO nanoparticles due incorporation of nanoparticles loaded on to potato peel. The broad absorption band observed around 3420 $cm^{-1}$. The O–H stretching vibrations associated with hydrogen-bonded hydroxyl groups, indicating the presence of surface –OH functionalities. In the case of the ZnO nanoparticles, prominent absorption peaks

were observed at 519 $cm^{-1}$ characteristics of Zn-O vibrations stretching. Similarly, the broad band centered at approximately 3420 $cm^{-1}$ is assigned to O-0H stretching vibrations, confirming the retention of hydroxyl groups after composite formation. Additionally, distinct peaks detected at lower wave numbers in ZnO@PP are characteristic of Zn-O stretching vibrations, thereby ensuring the effective integration of zinc oxide within the potato peel (Kataria and Garg, 2019; Saini et al., 2017).

### 3.3 FESEM and EDX Analysis of ZnO@PP nanocomposites

Scanning electron microscopy (SEM) was used to study the morphology structure and texture characteristics of the ZnO@PP nanoparticles at various magnification levels, as shown in Fig. 3.3. The micrographs indicate that the synthesized particles exhibit irregular shapes and are not perfectly spherical in nature. Energy-dispersive X-ray (EDX) investigation was carried out to study the composition of elements of the nanocomposite. The EDX spectrum confirms the presence of zinc and oxygen along with carbon as the major constituents, along with minor traces of other elements attributed to residual impurities, as illustrated in Fig. 3.4.

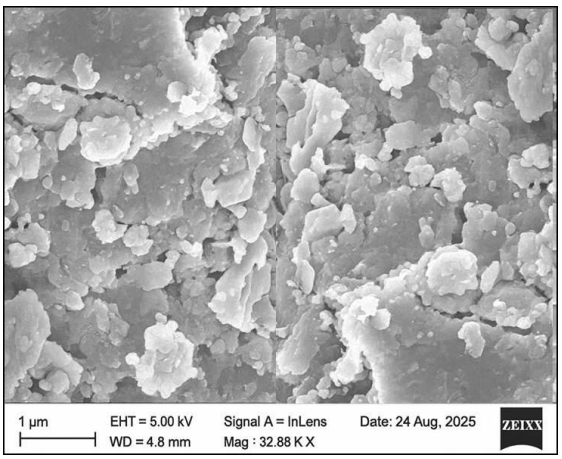


**Figure 3.3: FESEM Analysis of ZnO@Potato Peel Nanoparticles**

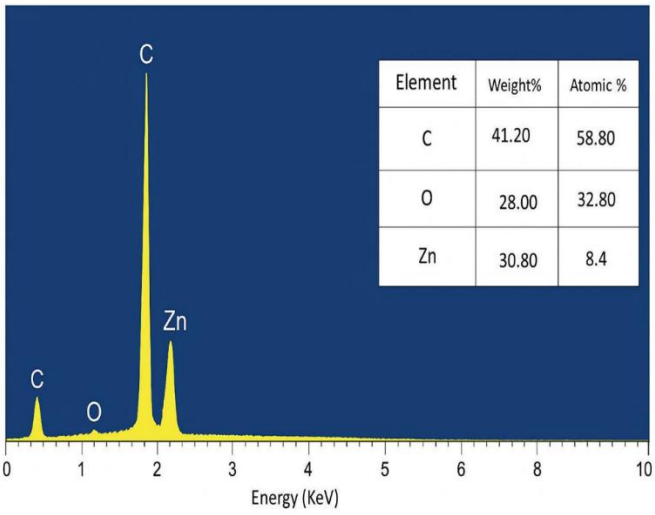


| Element | Weight% | Atomic % |
|---|---|---|
| C | 41.20 | 58.80 |
| O | 28.00 | 32.80 |
| Zn | 30.80 | 8.4 |

**Figure 3.4: Figure: EDX of ZnO@Potato Peel Nanoparticles**

## 4. Batch adsorption studies for dye removal from simulated water

Batch adsorption experiments were done to assess the efficiency of the synthesized adsorbent for eliminating cationic dyes from water. All experiments were carried out under dark conditions to exclude any photocatalytic influence. Key operational parameters-including initial dye concentration, solution pH, adsorbent dosage, and contact time-were systematically varied to determine their optimal values for maximum dye uptake

### 4.1 Effect of pH on dye removal

The influence of solution pH on the adsorption of the cationic dyes methylene blue (MB) and rhodamine B (RhB) was examined over a pH range of 2-10. The studies were performed using an adsorbent dose of 0.025 g per 50 mL of dye solution with the starting concentration of 50 $mg \cdot L^{-1}$, maintained at room temperature for 2hr contact time. With increase in pH from 2 to 10 resulted in a significant enhancement in efficiency of dye removal, rising from 73.88% to 96.22% for MB and from 71.85% to 94.21% for RhB using ZnO nanoparticles. While in case of ZnO loaded potato peel nanoparticles dye removal efficiency, rising from 79.87% to 99.46% for MB and from 75.86% to 98.04%, which is higher than ZnO nanoparticles. This behavior can be attributed to the reduced competition between hydrogen ions ($H^+$) and positively charged dye molecules at higher pH values, which facilitates stronger electrostatic interactions between the dyes and the adsorbent surface. The pH-dependent adsorption behavior of MB and RhB onto ZnO NPs and ZnO@PP nanoparticles is presented in Fig. 4.1a-b, respectively.

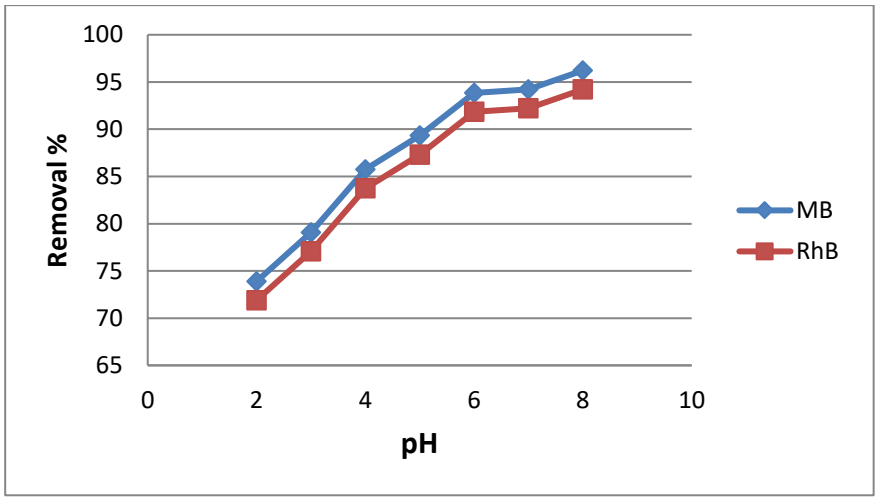


**Figure 4.1a: pH effect on the methylene blue and Rhodamine B dyes adsorption using ZnO nanoparticles.**

When the solution pH is lower than the surface of the adsorbent acquires a positive charge, which leads to electrostatic repulsion with the positively charged (cationic) dye molecules. As the pH increases, the adsorbent surface becomes negatively charged, thereby enhancing the electrostatic attraction toward cationic dye species. Simultaneously, the concentration of $H^+$ ions in the solution decreases markedly, resulting in reduced competition between hydrogen ions and dye cations for the available active adsorption sites (Liu et al., 2015; Kataria and Garg, 2019).

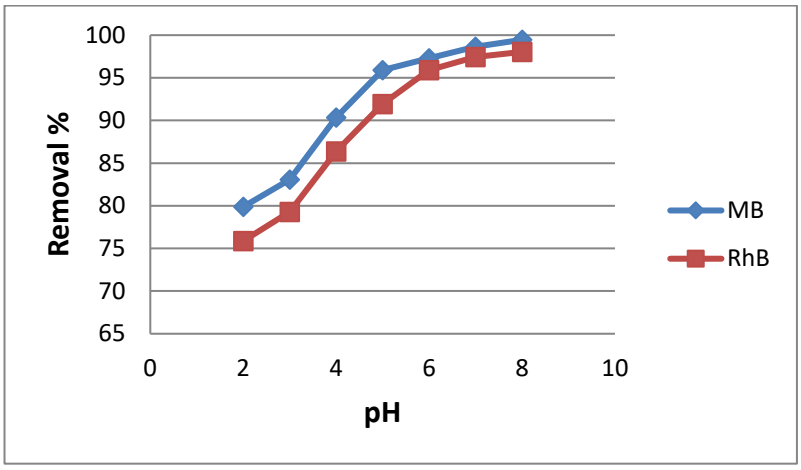


**Figure 4.1b: pH effect on the methylene blue and Rhodamine B dyes adsorption using ZnO@PP nanoparticles.**

The results clearly indicate that solution pH plays a crucial role in the adsorption process, as variations in pH influence both the adsorbate ionization state and adsorbent surface charge characteristics. At acidic pH values, stronger electrostatic repulsion between cationic dye molecules and the protonated adsorbent surface limits dye uptake, leading to lower removal efficiencies. In contrast, under alkaline conditions, the adsorbent surface carries a net negative charge, minimizing competition from $H^+$ ions and facilitating greater adsorption of cationic dyes. This pH-dependent adsorption behavior is consistent with earlier findings reported in earlier studies (Liu et al., 2015; Wu et al., 2016; Ali et al., 2017; Saini et al., 2018).

**4.2 Study the effect of dose concentration**

he adsorbent dosage effect on the uptake of cationic dyes was examined using solution of 50 mL dye with initial concentration of 50 $mg \cdot L^{-1}$ at room temperature and a contact time of 2 h. The adsorbent dose was varied between 0.01 and 0.04 g, as shown in Fig. 4.2 a-b. The removal efficiency increased steadily from 73.76% to 99.54% for MB dye while 69.54 to 98.84% for RhB using ZnO loaded potato peel nanoparticles with increasing adsorbent dosage. A similar trend was observed for ZnO Nanoparticle as adsorbent methylene blue (MB), where the removal efficiency rose 71.84% to 97.42% for MB dye while 67.34 to 96.64% for RhB Both dyes exhibited maximum adsorption at an adsorbent dose of 0.04 g, achieving complete dye removal. This improvement in adsorption performance can be attributed to the increased availability of active binding sites and a larger effective surface area at higher adsorbent dosages (Hem Lata et al., 2008; Wu et al., 2016; Jia et al., 2016; Kataria and Garg, 2017; Joshi et al., 2019). At a dosage of 0.04 g, the number of accessible adsorption sites becomes sufficient to effectively interact with and remove all cationic dye molecules present in the solution.

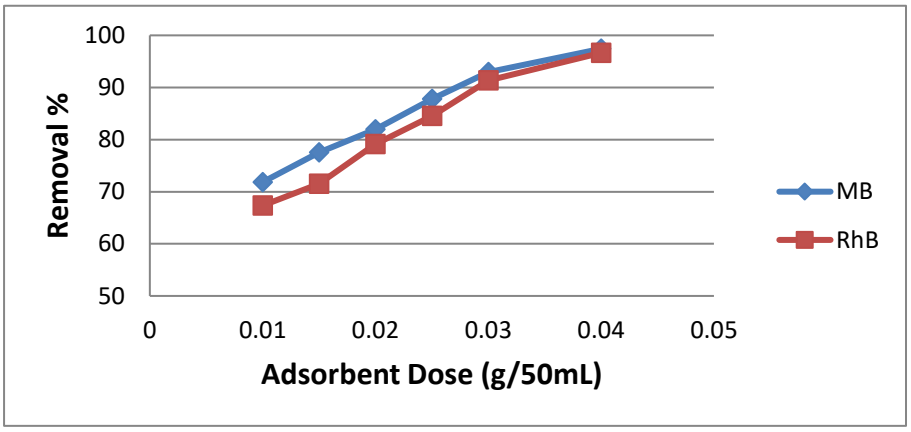


**Figure 4.2 a: Effect of adsorbent dose on removal of methylene blue (MB) and Rhodamine B (RhB) dyes using ZnO nanoparticles.**

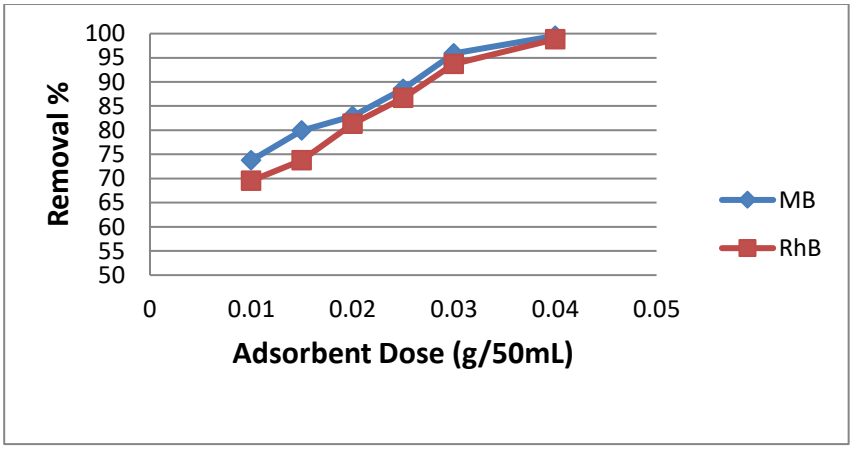


**Figure 4.2 b: Effect of adsorbant dose on removal of methylene blue (MB) and Rhodamine B (RhB) dyes using ZnO@PP nanoparticles.**

### 4.3 Initial dye concentration effect on dye removal

Figure 4.3 a,b illustrates the influence of the initial dye concentration, varied from 10 to 100 mg/L, on the removal efficiency of cationic dyes. It is evident from the figure that the percentage removal of dye decreases as the initial dye concentration increases. At a lower concentration of 10 mg/L, removal (99.5%) was achieved for methylene blue (MB) and 98.3% for rhodamine B (Rh B). However, when the concentration was increased to 100 mg/L, the removal efficiency declined to 69.88% for MB and 68.07% for Rh B. This reduction in removal efficiency at higher dye concentrations can be attributed to the availability of a greater number of vacant and active adsorption sites on the adsorbent surface at low concentrations, which facilitates efficient dye uptake. In contrast, at higher concentrations, the fixed number of active binding sites becomes progressively occupied, leading to surface saturation and limited interaction between dye molecules and the adsorbent. Consequently, the overall dye removal efficiency decreases with increasing initial dye concentration (Liu et al., 2015; Wu et al., 2016; Saini et al., 2018).

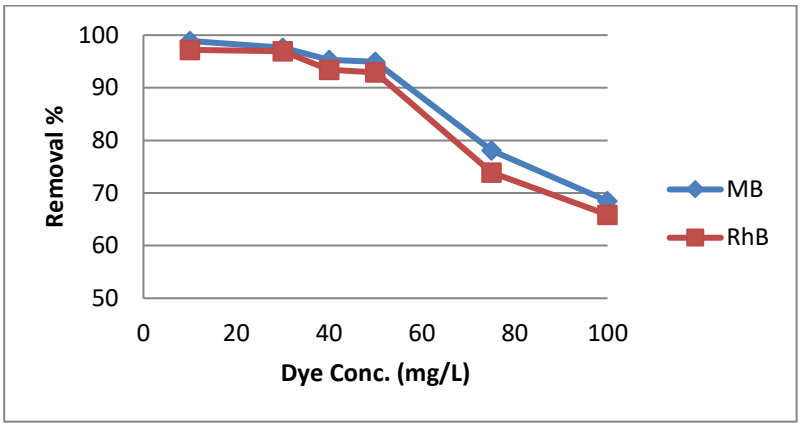


**Fig 4.3 a: Effect of dye concentration on adsorption of MB and RhB dyes on ZnO nanoparticles**

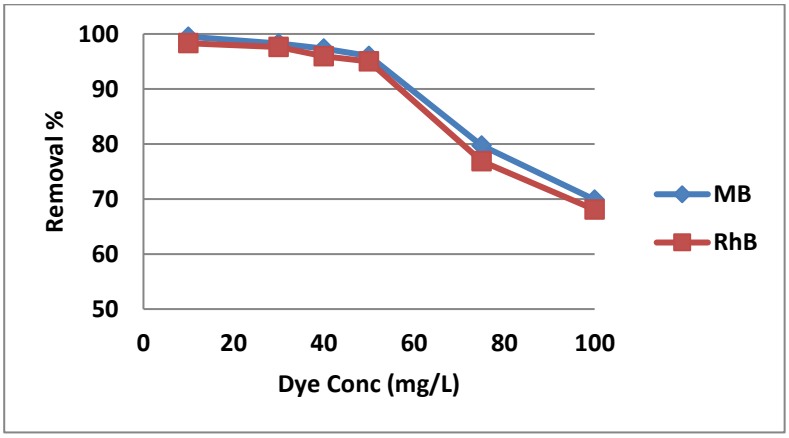


**Fig 4.3 b: Effect of dye concentration on adsorption of MB and RhB dyes on ZnO potato peel loaded (ZnO@PP) nanoparticles.**

### 4.4 Effect of Contact Time on Dye Removal

Figures 4.4 (a,b) and 4.4 (c,d) illustrate the influence of contact time on the removal of methylene blue (MB) and Rhodamine dyes, with the contact duration varied from 0 to 120 minutes. Batch adsorption experiments were performed in 250 mL Erlenmeyer flasks containing 50 mL of dye solutions with initial concentrations ranging from 30 to 100 mg/L. An adsorbent dose of 0.025 g per 50 mL was used, and the experiments were carried out at a controlled temperature of 27 ± 1 °C.

A rapid increase in dye adsorption was observed during the initial stage, than increase with time for both ZnO nanoparticles and ZnO loaded potato peel nanoparticles. This rapid uptake can be attributed to the presence of a large number of readily available active sites on the adsorbent surface. Beyond this period, the rate of adsorption gradually decreased, showing only a marginal increase in dye removal, and equilibrium was eventually reached at around 120 minutes. This behavior indicates that most of the accessible adsorption sites became occupied by dye molecules, leaving no additional active sites available for further adsorption (Liu et al., 2015; Duman et al., 2016; Kataria and Garg, 2019).

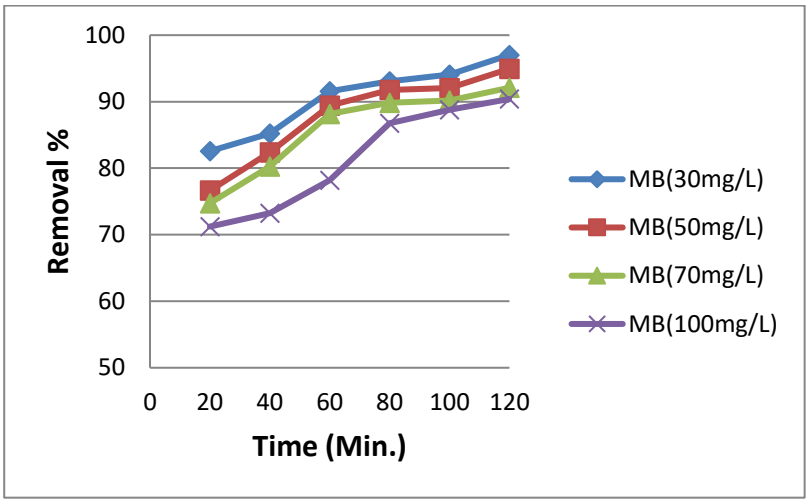


**Fig. 4.4 a: Effect of contact time on adsorption of MB on ZnO@PP nanoparticles**

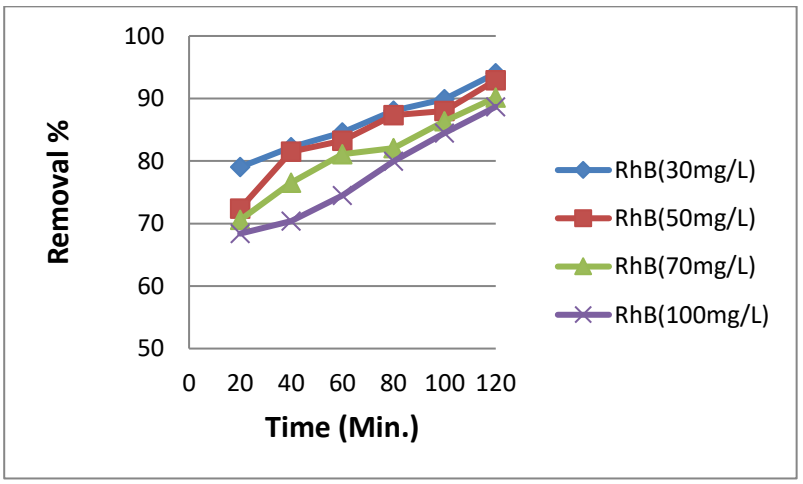


**Fig. 4.4 b: Effect of contact time on adsorption of RhB on ZnO@PP nanoparticles**

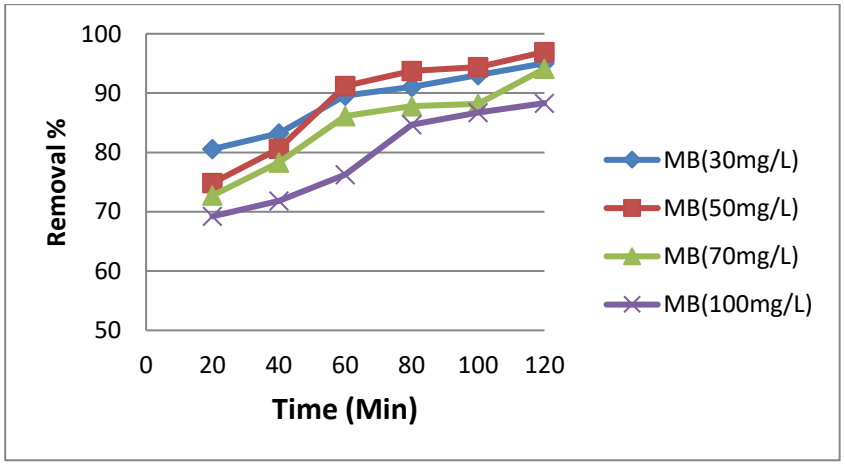


**Fig. 4.4 c: Effect of contact time on adsorption of MB on ZnO nanoparticles**

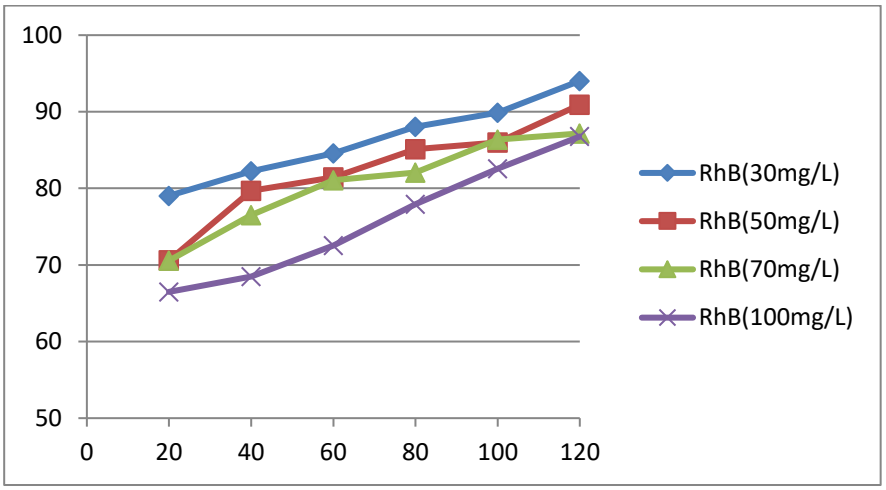


**Fig. 4.5 d: Effect of contact time on adsorption of RhB on ZnO nanoparticles**

### 4.5 Effect of temperature on dye removal

The influence of temperature on the adsorption of methylene blue (MB) and Rhodamine B (RhB) dyes was investigated over a temperature range of 10-50 °C at a fixed dye concentration of 50 mg/L and a contact time of 120 minutes. As depicted in Fig. 4.10a,b both dyes exhibited a similar response to changes in temperature. An increase in temperature led to a noticeable improvement in dye removal efficiency, with MB removal rising from 80% to 96.13% and with RhB removal increasing from 76.94% to 93.5% using ZnO@PP as adsorbent while with MB removal rising from 78% to 94.13% and with RhB removal increasing from 74.94% to 91.5% using ZnO as adsorbent. This enhancement in adsorption performance with increasing temperature can be attributed to improved interaction between dye molecules and the active sites on the adsorbent surface. Higher temperatures increase the kinetic energy of dye molecules, thereby enhancing their mobility and diffusion within the aqueous phase and facilitating greater access to adsorption sites. Based on these observations, the adsorption studies were subsequently carried out at room temperature, in agreement with earlier reports (Liu et al., 2015; Altıntıg et al, 2017).

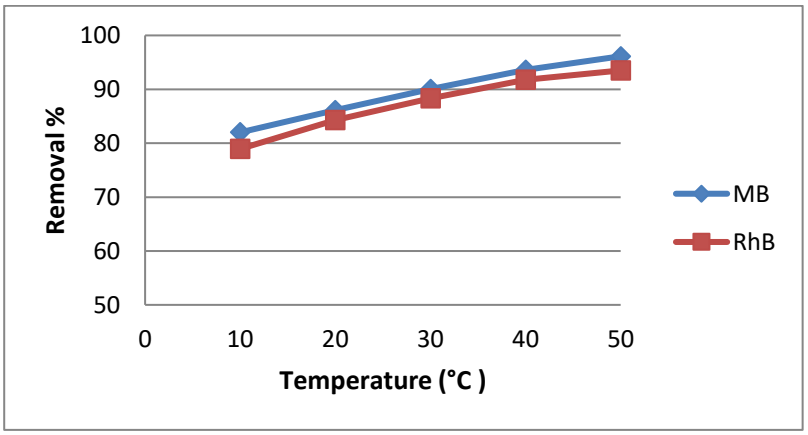


**Fig. 4.5 a: Effect of temperature on adsorption of MB and RhB on ZnO@PP nanoparticles**

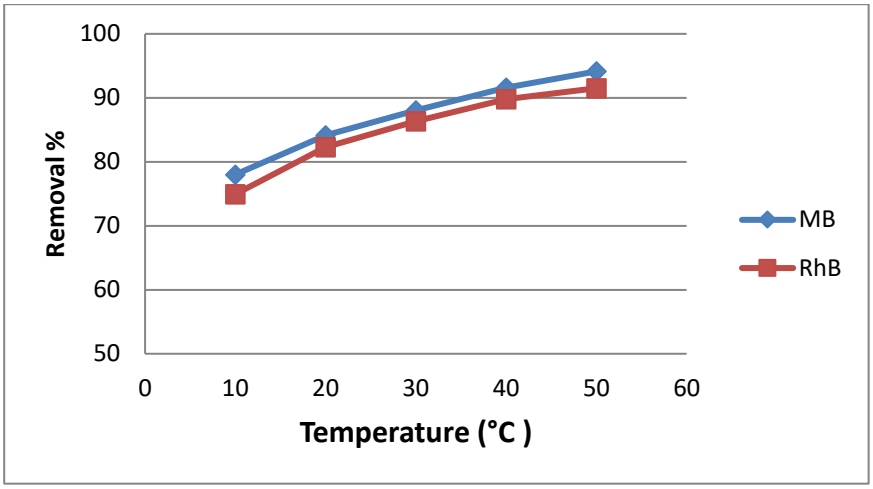


**Fig. 4.5 b: Effect of temperature on adsorption of MB and RhB on ZnO nanoparticles**

### 4.6 Thermodynamic behaviour study

Thermodynamic parameters, including changes in standard entropy (ΔS°), Gibbs free energy (ΔG°), and enthalpy (ΔH°), for the adsorption of cationic dyes onto ZnO@PP nanoparticles were evaluated through experiments conducted at different temperatures. These parameters were determined using established thermodynamic relationships, as reported in the literature (Saini et al., 2018). The corresponding equations employed for the analysis are given below:

$$\Delta G^0 = -RTlnK_d \quad (1)$$

$$K_d = \frac{C_a}{C_e} \quad (2)$$

$$lnK_d = -\frac{\Delta H^0}{RT} + \frac{\Delta S^0}{R} \quad (3)$$

Here, Kd represents the equilibrium constant, R is the universal gas constant (8.314 J $mol^{-1}$ $K^{-1}$), and T (K) denotes the absolute temperature. The term (mg/L) corresponds to the amount of MB and Rh B dyes adsorbed onto the nanoadsorbent surface at equilibrium. The values of standard enthalpy change (ΔH°) and standard entropy change (ΔS°) were calculated from the slope and intercept, respectively, of the linear plots of lnKd versus 1/T1 (Fig. 4.6 a-d).

As summarized in Table 4.1, the positive ΔH° values for both dyes indicate that the adsorption process is endothermic in nature, suggesting that the uptake of MB and RhB occurs predominantly through a physical adsorption mechanism (Liu et al., 2015; Kataria and Garg, 2017). Furthermore, the positive ΔS° values-125.12 J

$mol^{-1}$ $K^{-1}$ for MB and 122.42 J $mol^{-1}$ $K^{-1}$ for MB and RhB dyes by ZnO@PP and 110.55 J $mol^{-1}$ $K^{-1}$ for MB and 95.70 J $mol^{-1}$ $K^{-1}$ for MB and RhB dyes by ZnO@PP -reflect an increase in randomness and mobility at the solid–solution interface, which favors the adsorption of dye molecules. The negative values of ΔG° for both MB and Rh B confirm that the adsorption process is thermodynamically feasible and spontaneous under the studied conditions, as presented in Table 4.1 and table 4.2.

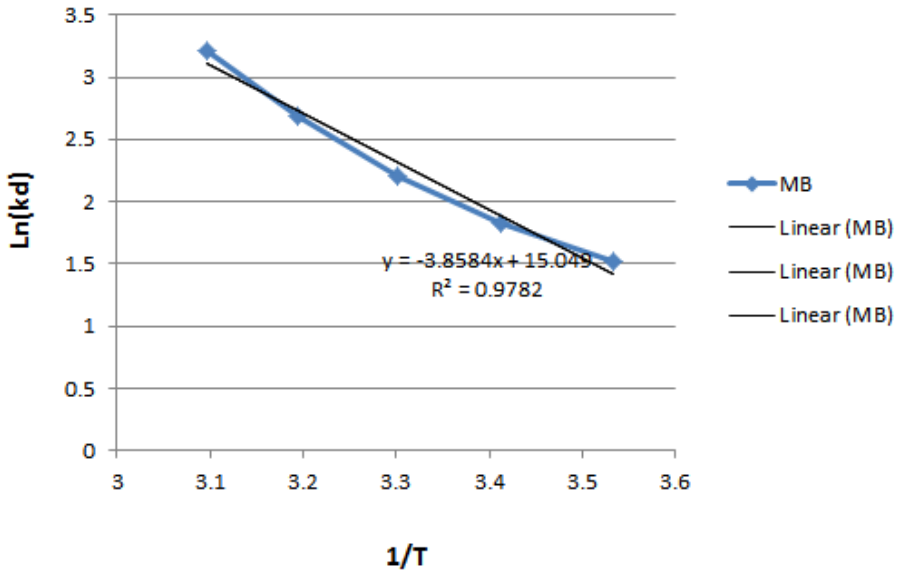


**Fig 4.6 a: Thermodynamic plot for MB dye removal by ZnO@PP nanoparticles**

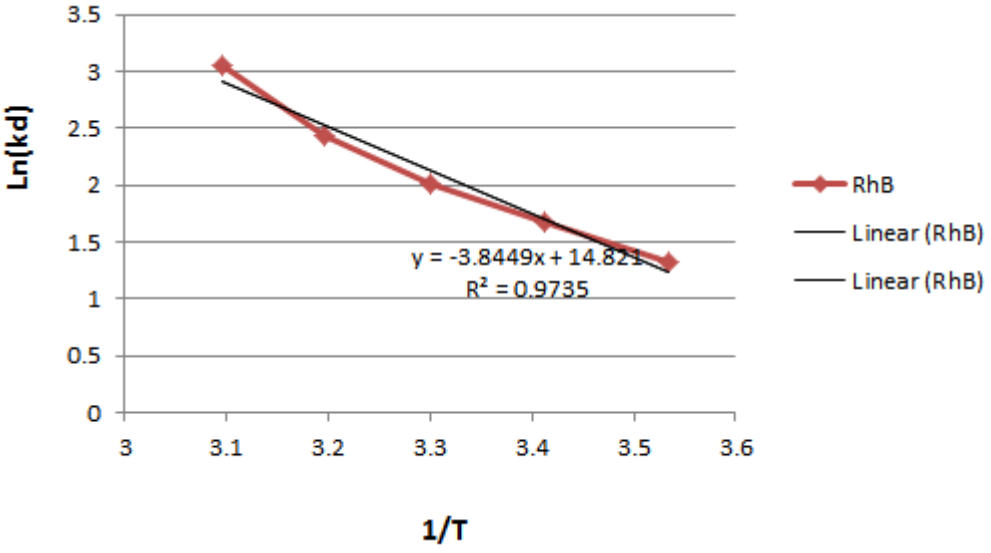


**Fig 4.6 b: Thermodynamic plot for RhB dye removal by ZnO@PP nanoparticles**

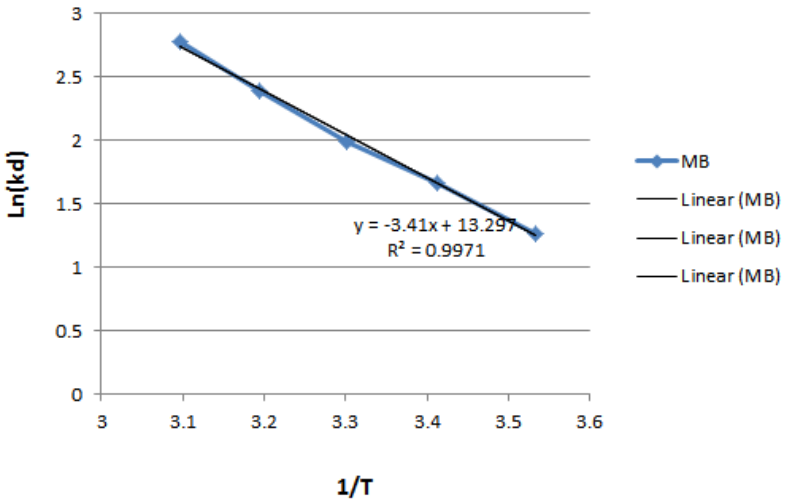


**Fig 4.6 c: Thermodynamic plot for MB dye removal by ZnO nanoparticles**

**Table 4.1: Thermodynamic parameters for the adsorption of MB and RhB dyes onto ZnO@PP**

| Temperature (K) | ΔG° for MB (kJ mol⁻¹) | ΔS° for MB (J mol⁻¹ K⁻¹) | ΔH° for MB (kJ mol⁻¹) | ΔG° for RhB (kJ mol⁻¹) | ΔS° for RhB (J mol⁻¹ K⁻¹) | ΔH° for RhB (kJ mol⁻¹) |
|---|---|---|---|---|---|---|
| 283 | -3.57 | 125.12 | 32.08 | -3.11 | 122.42 | 31.74 |
| 293 | -4.46 | — | — | -4.10 | — | — |
| 303 | -5.55 | — | — | -5.10 | — | — |
| 313 | -6.97 | — | — | -6.27 | — | — |
| 323 | -8.61 | — | — | -8.19 | — | — |

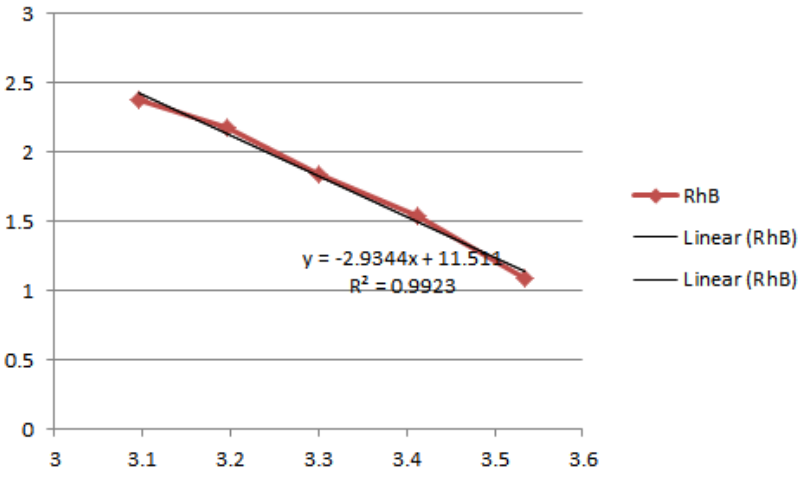


**Fig 4.6 d: Thermodynamic plot for RhB dye removal by ZnO nanoparticles**

**Table 4.2: Thermodynamic parameters for the adsorption of MB and RhB dyes onto ZnO**

| Temperature (K) | ΔG° for MB (kJ mol⁻¹) | ΔS° for MB (J mol⁻¹ K⁻¹) | ΔH° for MB (kJ mol⁻¹) | ΔG° for RhB (kJ mol⁻¹) | ΔS° for RhB (J mol⁻¹ K⁻¹) | ΔH° for RhB (kJ mol⁻¹) |
|---|---|---|---|---|---|---|
| 283 | -2.98 | 110.55 | 28.35 | -2.58 | 95.70 | 24.40 |
| 293 | -4.07 | — | — | -3.74 | — | — |
| 303 | -5.03 | — | — | -4.64 | — | — |
| 313 | -6.21 | — | — | -5.65 | — | — |
| 323 | -7.45 | — | — | -6.38 | — | — |

### 4.7 Kinetic study

The adsorption kinetics of cationic dyes onto the synthesized ZnO@PP nanoadsorbents were systematically examined by the pseudo-first-order kinetic model originally proposed by Lagergren (1898) and the pseudo-second-order kinetic model developed by McKay and Ho (1999). These models were applied to quantitatively describe the adsorption rate behavior and to identify the dominant rate-controlling mechanisms governing the adsorption process. The linearized forms of the pseudo-first-order and pseudo-second-order kinetic equations are presented as follows:

$$\log(q_e - q_t) = \log q_e - \left(\frac{k_1}{2.303}\right) t \quad (4)$$

$$t/q_t = 1/k_2 q_e^2 + t/q_e \quad (5)$$

$$q_t = k_{id} t^{1/2} + C \quad (6)$$

Where qe(mg $g^{-1}$) represents the adsorption capacity at equilibrium and qt(mg $g^{-1}$) denotes the adsorption capacity at any time t. The rate constants k1 ($min^{-1}$) and k2 (g $mg^{-1}$ $min^{-1}$) correspond to the pseudo-first-order and pseudo-second-order kinetic models, respectively. The kinetic parameters obtained from both models are concluded in Table 4.3 and were evaluated by fitting the experimental data to the linearized forms of the respective kinetic equations using linear regression analysis. Figures 4.7 (a–d) illustrate the plots associated with the pseudo-first-order and pseudo-second-order models. For the pseudo-first-order model, the parameters k1 and qe were determined from the slope and intercept of the plot of log(qe-qt) versus t, whereas for the pseudo-second-order

model, these parameters were obtained from the linear plot of t/qt versus t. The calculated equilibrium adsorption capacities qe(cal) derived from the pseudo-first-order model were consistently lower than the experimentally determined values qe-(exp) for both cationic dyes, indicating a poor fit of this model to the experimental data. In contrast, the pseudo-second-order model exhibited significantly higher regression coefficients (R2=0.999) for both dyes, along with a close agreement between qe(cal) and qe (exp). These findings clearly demonstrate that the adsorption kinetics of both cationic dyes onto Zno@PP nanoparticles are better described by the pseudo-second-order kinetic model, signifying that the adsorption method is predominantly governed by chemisorption mechanisms comprising valence forces over electron sharing or exchange.

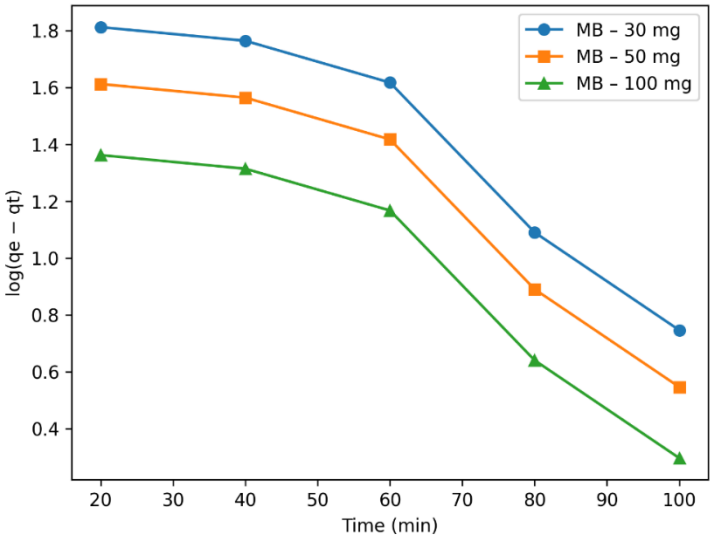


**Fig 4.7: (a) Comparative Pseudo first order plot for MB dye on ZnO@PP nanoparticles**

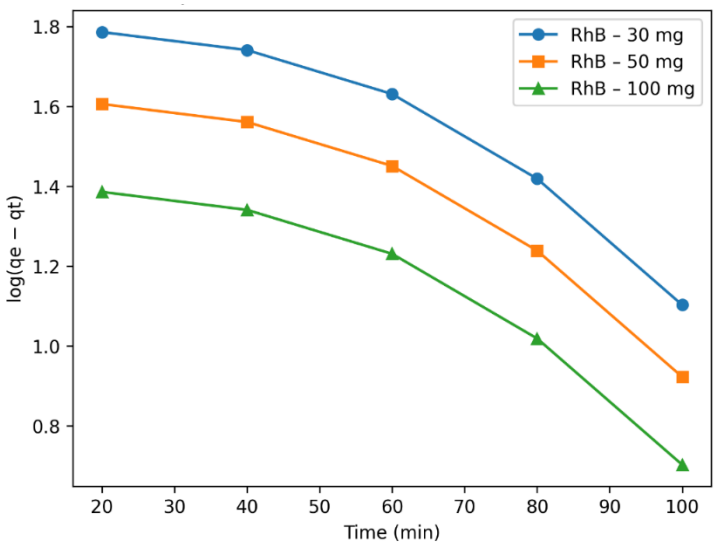


**Fig 4.7: ( b) Comparative Pseudo first order plot for RhB dye on ZnO@PP nanoparticles**

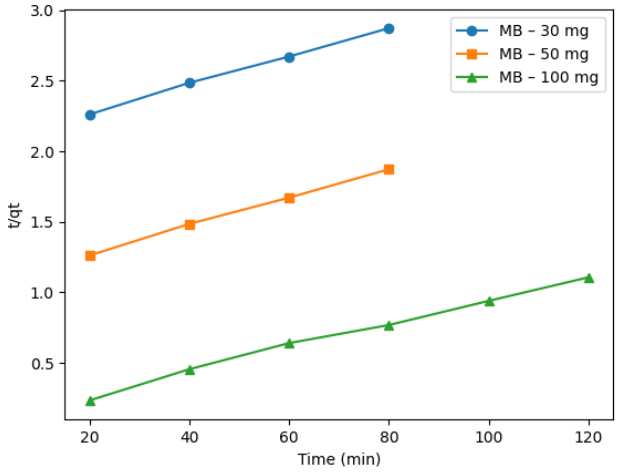


**Fig 4.7: (c) Comparative Pseudo Second order plot for MB dye on ZnO@PP nanoparticles**

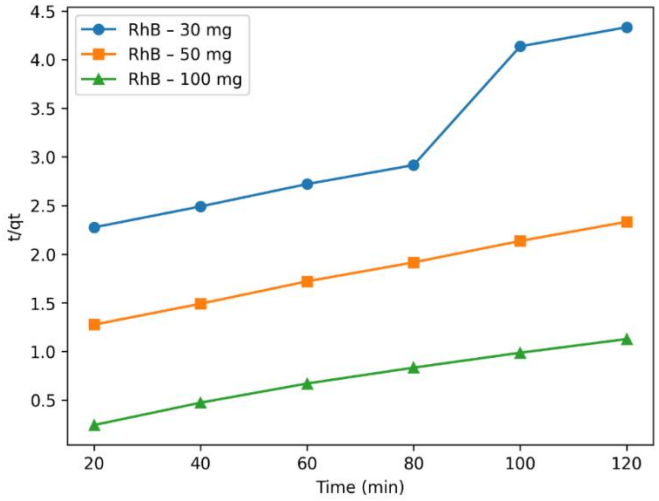


**Fig 4.7: (d) Comparative Pseudo Second order plot for Rh dye on ZnO@PP nanoparticles**

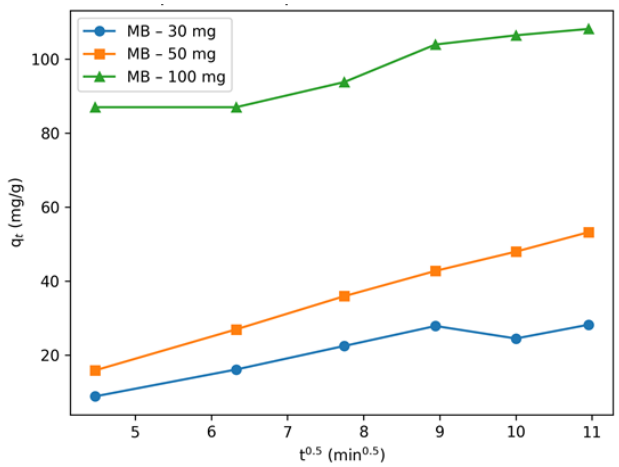


**Fig 4.7: (e) Comparative Intraparticle Diffusion Model for MB dye on ZnO@PP nanoparticles**

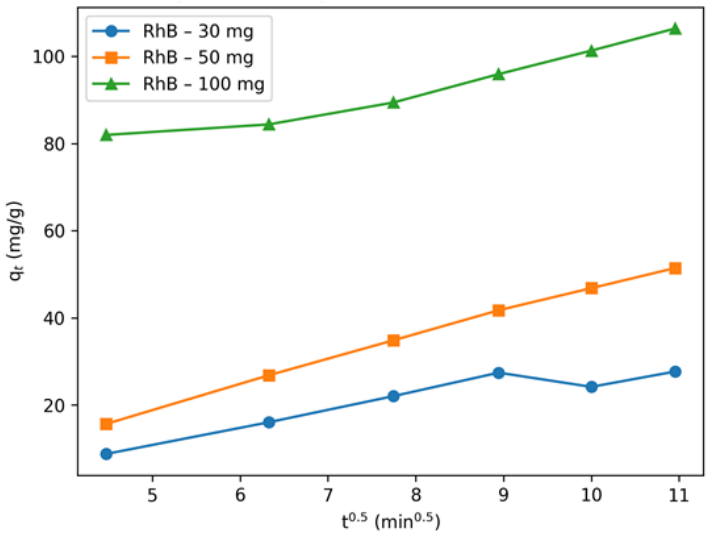


**Fig 4.7: (f) Comparative Intraparticle Diffusion Model for RhB dye on ZnO@PP nanoparticle**

In the intraparticle diffusion model, kid represents the intraparticle diffusion rate constant, while C denotes the intercept associated with the thickness of the boundary layer surrounding the adsorbent particles. The values of kid and C were determined from the slope and intercept, respectively, of the linear plots of qt versus t1/2. This model assumes that the adsorption of both cationic dyes (MB and RhB) proceeds via the transport of dye molecules from the bulk solution to the internal pores of the adsorbent through an external boundary layer (Liu et al., 2015; Kataria and Garg, 2019; Wolski,et al., 2024).

**Table 4.3: Description of kinetic models parameters of MB and Rh B dyes adsorption**

| Kinetic Model | Parameter | MB 30 mg/L | MB 50 mg/L | MB 100 mg/L | RhB 30 mg/L | RhB 50 mg/L | RhB 100 mg/L |
|---|---|---|---|---|---|---|---|
| **Pseudo-first-order** | $K_1$ ($min^{-1}$) | 0.034 | 0.0242 | 0.0331 | 0.036 | 0.025 | 0.019 |
| | $q_e$(cal) | 28.20 | 53.19 | 108.11 | 27.69 | 51.44 | 106.38 |
| **Pseudo-second-order** | $k_2$ (g $mg^{-1}$ $min^{-1}$) | 0.028 | 0.093 | 0.077 | 0.003 | 0.110 | 0.069 |
| | $q_e$(cal) | 46.73 | 100.30 | 117.15 | 45.41 | 94.40 | 114.34 |
| | $R^2$ | 0.884 | 0.999 | 0.994 | 0.891 | 0.999 | 0.991 |
| **Intraparticle diffusion — Stage I** | $k_i$d(I) (mg $g^{-1}$ $min^{-1/2}$) | 2.95 | 5.77 | 3.84 | 2.88 | 5.53 | 3.91 |
| | C(I) | 64.20 | 65.90 | 66.70 | 23.10 | 60.40 | 61.64 |
| | $R^2$(I) | 0.885 | 0.999 | 0.908 | 0.886 | 0.998 | 0.951 |

| | | | | | | | |
|---|---|---|---|---|---|---|---|
| **Intraparticle diffusion — Stage II** | $k_i d$(II) (mg $g^{-1}$ $min^{-1/2}$) | — | 1.74 | 7.89 | 0.56 | 1.90 | 1.29 |
| | C(II) | — | 74.75 | 53.42 | 53.18 | 68.36 | 151.00 |
| | $R^2$(II) | — | 0.896 | 0.948 | 0.805 | 0.984 | 0.899 |
| **Experimental data** | $q_e$(exp) | 34.93 | 58.55 | 105.97 | 33.85 | 54.16 | 104.12 |
| | $R^2$ | 0.478 | 0.982 | 0.883 | 0.460 | 0.978 | 0.908 |

As presented in Table 4.3, the relatively higher values of the intercept C obtained for both MB and RhB dyes indicate a significant contribution of boundary layer diffusion during the adsorption process. Furthermore, the presence of two distinct linear regions in the intraparticle diffusion plots (Fig. 4.7 (e, f)) suggests a multi-step adsorption mechanism. The initial linear portion corresponds to the rapid migration of dye molecules from the bulk solution to the external surface of the adsorbent, whereas the subsequent linear region is attributed to intraparticle diffusion within the pores, followed by attainment of equilibrium. These observations imply that the overall adsorption kinetics of cationic dyes onto the adsorbents is governed by a combined effect of boundary layer diffusion and intraparticle diffusion.

### 4.8 Equilibrium isotherm models

The adsorption behavior and the nature of interactions between the adsorbent surface and dye molecules were analyzed using adsorption isotherm models. To elucidate the equilibrium characteristics of cationic dye adsorption onto ZnO@ PP nanoparticles, the Langmuir, Freundlich, Temkin, and Dubinin–Radushkevich (D–R) isotherm models were fitted to the experimental adsorption data. These models provide insight into surface heterogeneity, adsorption capacity, and the energetics of the adsorption process. The linearized form of the Langmuir isotherm model is expressed as follows.

$$\frac{C_e}{q_e} = \frac{1}{q_{max} b} + \frac{C_e}{q_{max}} \quad (7)$$

Where $b$ (L/mg) is the Langmuir constant, $q_{max}$ (mg/g) is the maximum monolayer adsorption capacity.

Freundlich isotherms model (Freundlich, 1906) may be represented by the equation:

$$\log q_e = \log K_f + \frac{1}{n} \log C_e \quad (8)$$

In the Freundlich isotherm model, Kf represents the Freundlich constant associated with the adsorption capacity of the adsorbent, while 1/n is the heterogeneity factor that reflects the adsorption intensity and surface heterogeneity. For a favorable adsorption process, the value of 1/n should lie between 0 and 1. A value of 1/n proaching zero indicates a highly heterogeneous adsorbent surface, whereas 1/n suggests that the adsorption process is predominantly chemisorptive in nature. Conversely, values of 1/n are indicative of cooperative adsorption behavior (Liu et al., 2015; Kataria and Garg, 2019; Wolski,et al., 2024).

The Temkin–Pyzhev isotherm model (Temkin and Pyzhev, 1940), which accounts for adsorbent–adsorbate interactions and assumes a linear decrease in the heat of adsorption with surface coverage, is expressed as:

$$qe=BlnKT+BlnKe$$

Where R (8.314 J $mol^{-1}$ $K^{-1}$) is the universal gas constant, T (K) is the absolute temperature, and B=RT, with b (J $mol^{-1}$) representing the Temkin constant related to the heat of adsorption. The parameter KT(L $g^{-1}$) denotes the Temkin equilibrium binding constant. The isotherm model parameters and corresponding correlation coefficients for MB and RhB dyes are summarized in Table 4.4, while the linearized plots of the Langmuir, Freundlich, and Temkin isotherm models are illustrated in Fig. 4.8 (a–c). Among the evaluated models, the Langmuir isotherm exhibited the highest correlation coefficients, with R2=0.943R for MB dye and R2=0.910 for RhB dye, indicating superior fitting compared to the Freundlich and Temkin models. This observation suggests that the adsorption of both cationic dyes onto ZnO@PP nanoparticles occurs predominantly via monolayer formation on a homogeneous surface. The maximum monolayer adsorption capacities qmax for MB and RhB dyes were determined to be 108 mg $g^{-1}$ and 106 mg $g^{-1}$, respectively. A comparative evaluation of the adsorption capacities of MB and RhB dyes described for various adsorbents is presented in Table 4.5. The relatively high adsorption capacities obtained in the present study demonstrate that ZnO@PP nanoparticles are promising and efficient adsorbents for the removal of cationic dyes from simulated wastewater systems.

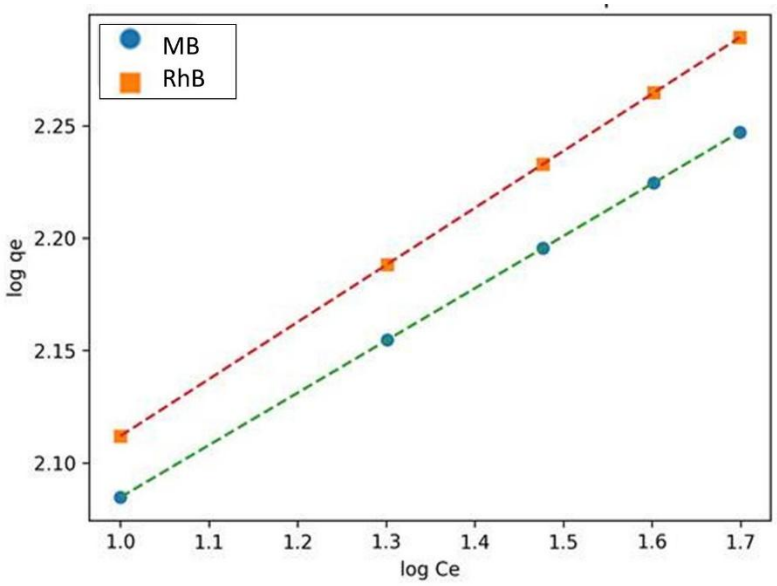

**Fig 4.14: (a) Langmuir isotherm Adsorption isotherm plots for MB and RhB dyes removal by ZnO@PP nanoparticles**

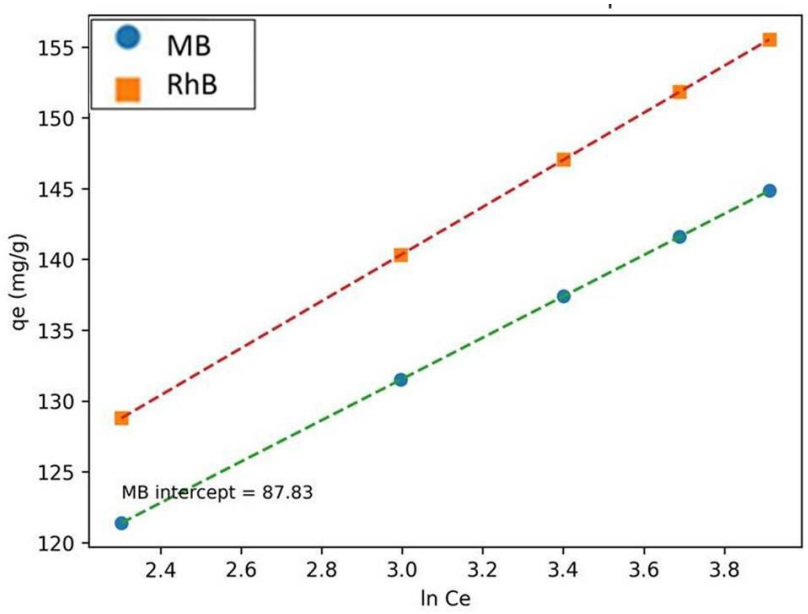


**Fig 4.8: (b) Freundlich isotherm Adsorption isotherm plots for MB and RhB dyes removal by ZnO@PP nanoparticle**

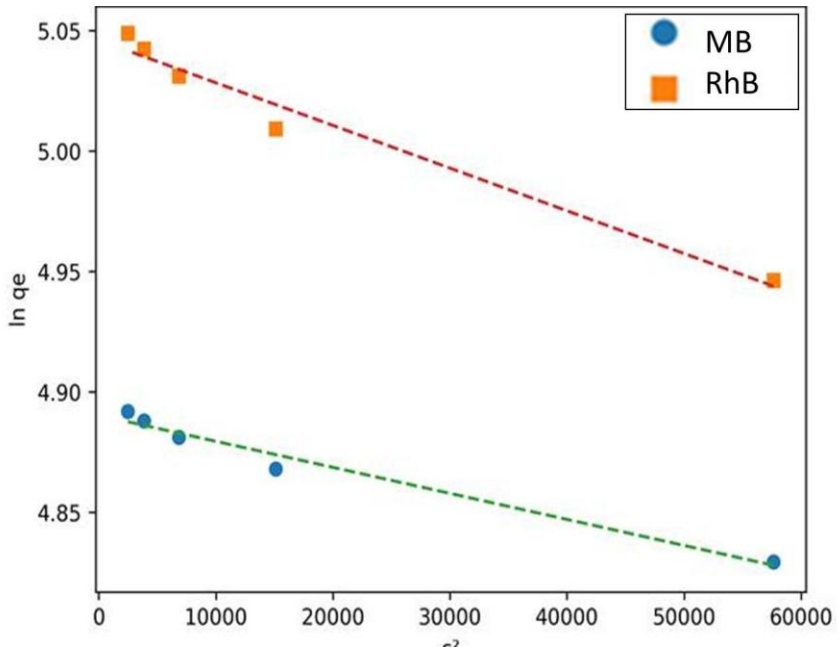


**Fig 4.8: (c) Temkin and Pyzhev Adsorption isotherm plots for MB and RhB dyes removal by ZnO@PP nanoparticles**

**Table 4.4: Description of adsorption isotherms model parameters of methylene blue and Rh B dyes adsorption**

| Isotherm Model | Parameter | Methylene Blue | Rhodamine B |
|---|---|---|---|
| **Langmuir** | qmax (mg/g) | 135.4 | 160.2 |
| | b (L/mg) | 1.22 | 0.72 |
| | $R^2$ | 0.943 | 0.910 |
| **Freundlich** | 1/n | 0.232 | 0.253 |
| | Kf (mg/g) | 71.14 | 72.13 |
| | $R^2$ | 0.903 | 0.892 |
| **Temkin and Pyzhev** | bT | 172.8 | 151.6 |
| | KT (L/mg) | 413.4 | 232.4 |
| | $R^2$ | 0.872 | 0.708 |

**Table 4.5: Reported maximum adsorption capacities of different adsorbent materials for methylene blue (MB) and Rhodamine B (RhB) dyes**

| Sl. No. | Adsorbent Material | Target Dye | Maximum Adsorption Capacity, qmax (mg $g^{-1}$) | Source |
|---|---|---|---|---|
| 1 | Tea waste–derived adsorbent | MB | 85.16 | Uddin et al., 2009 |
| 2 | Magnetic biochar | MB | 31.25 | Mubarak et al., 2015 |
| 3 | Mt/PANI/$Fe_3O_4$ nanocomposite | MB | 184.50 | Mu et al., 2016 |
| 4 | $Fe_3O_4$–graphene@mesoporous $SiO_2$ | MB | 139.00 | Wu et al., 2016 |
| 5 | PPy/$Al_2O_3$ composite | MB | 134.77 | Chen et al., 2016 |

| | | | | |
|---|---|---|---|---|
| 6 | $Fe_3O_4$–charcoal nanocomposite | MB | 97.50 | Albadarin et al., 2014 |
| 7 | $Fe_3O_4$@Ag/$SiO_2$ | MB | 128.40 | Saini et al., 2018 |
| 8 | ZnO@AC nanoparticles | MB | 32.20 | Nourmoradi et al., 2015 |
| 9 | Ag nanoparticle–loaded activated carbon | MB | 71.40 | Ghaedi et al., 2012 |
| 10 | Pd nanoparticle–loaded activated carbon | MB | 75.40 | Ghaedi et al., 2012 |
| 11 | Au nanoparticle–loaded activated carbon | MB | 185.00 | Rouhi et al., 2019 |
| 12 | Acid-treated activated carbon | MB | 60.60 | Ali et al., 2017 |
| 13 | ZnO@PP | MB | 108.00 | Current study |
| 14 | Parthenium-derived carbon | Rhodamine B | 18.52 | Hem Lata et al., 2008 |
| 15 | Activated carbon from industrial waste | Rhodamine B | 16.12 | Kadirvelu et al., 2005 |
| 16 | Natural adsorbent (*Argemone mexicana*) | Rhodamine B | 6.40 | Khamparia et al., 2016 |
| 17 | $Fe_3O_4$/HA composite | Rhodamine B | 161.80 | Peng et al., 2012 |
| 18 | Ag@AgBr/SBA-15 nanocomposite | Rhodamine B | 66.67 | Hu et al., 2015 |
| 19 | Magnetic bentonite ($Fe_3O_4$/Al-B) | Rhodamine B | 62.15 | Wan et al., 2015 |
| 20 | ZnO@PP | Rhodamine B | 106.00 | Current study |

### 4.9 Reuse Potential of nanoadsorbent

In the present study, the reusability and regeneration efficiency of ZnO@PP nanoparticles were evaluated, four consecutive adsorption–desorption cycles, as illustrated in Fig. 4.9. After completion of each adsorption experiment, the spent adsorbent was recovered from the aqueous phase by centrifugation. The separated material was subsequently washed repeatedly with ethanol followed by distilled water to remove residual dye molecules and then dried in an oven at 80 °C for several hours. The regenerated ZnO@PP nanoparticles were reused for subsequent adsorption cycles of cationic dyes.

During the first adsorption cycle, the removal efficiencies were found to be 97.42% for RhB dye and 96.62% for MB dye. A marginal decline in dye removal efficiency was observed after the third cycle for both dyes, after which the removal percentages remained nearly constant in the fourth cycle, as shown in Fig. 4.9. These results indicate that ZnO@PP nanoparticles exhibit good structural stability and regeneration capability, demonstrating their potential for repeated use in the removal of cationic dyes from aqueous systems.

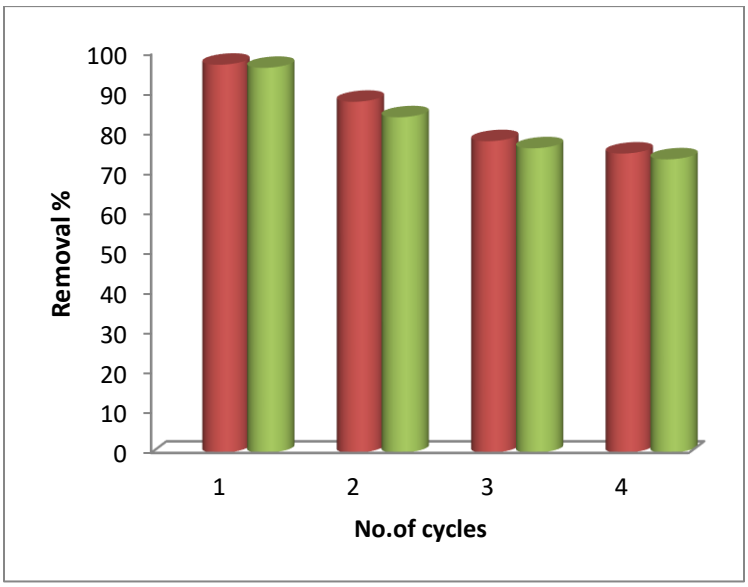


**Fig 4.9: Reuse potential of ZnO@PP NPs for MB and RhB dyes**

### 5. Conclusions

In this work, ZnO and ZnO@PP nanoparticles were synthesized successfully using a co-precipitation approach and exhibited remarkable adsorption capability for cationic dyes under optimized conditions. When compared with previously reported nanoadsorbent materials, the prepared ZnO@PP showed enhanced efficiency for the removal of cationic dyes from aqueous solutions. The highest adsorption capacities achieved were 108 mg $g^{-1}$ for methylene blue (MB) and 106 mg $g^{-1}$ for Rhodamine B (RhB). Analysis of equilibrium data revealed a good fit with the Langmuir isotherm model, suggesting uniform monolayer adsorption on a homogeneous surface. Kinetic investigations indicated that the adsorption behavior of both dyes followed a pseudo-second-order model, implying that chemisorption is the

dominant controlling mechanism. In addition, regeneration studies demonstrated that the ZnO@PP nanoparticles maintained significant adsorption performance over several reuse cycles, confirming their structural stability and reusability. Overall, the results establish ZnO@PP nanoparticles as effective and sustainable nanoadsorbents for the removal of cationic dyes from water systems.

**Conflicts of interest**

There are no conflicts to declare.

**References:**


- Ahmad, A., Mohd-Setapar, S. H., Chuong, C. S., et al. (2015). Recent advances in new generation dye removal technologies: Novel search for approaches to reprocess wastewater. RSC Advances, 5, 30801–30818. https://doi.org/10.1039/C4RA16959J
- Ahmed, S., Ahmad, M., Swami, B. L., & Ikram, S. (2016). A review on plant extract-mediated synthesis of silver nanoparticles for antimicrobial applications: A green expertise. *Journal of Advanced Research, 7*(1), 17–28.
- Akcil, A., & Koldas, S. (2006). Acid mine drainage (AMD): Causes, treatment and case studies. *Journal of Cleaner Production, 14*(12–13), 1139–1145. https://doi.org/10.1016/j.jclepro.2005.11.011
- Albadarin, A. B., Mo, J., Glocheux, Y., Allen, S., Walker, G., & Mangwandi, C. (2014). Preliminary investigation of mixed adsorbents for the removal of copper and methylene blue from aqueous solutions. Chemical Engineering Journal, 255, 525–534.
- Ali, A. F., Kovo, A. S., & Adetunji, S. A. (2017). Removal of methylene blue and brilliant green dyes from aqueous solution using agricultural waste–derived activated carbon. Journal of Encapsulation and Adsorption Sciences, 7(2), 95–104.
- Altıntıg, E., Altundağ, H., Tuzen, M., & Sarı, A. (2017). Effective removal of methylene blue from aqueous solutions using magnetic-loaded activated carbon as a novel adsorbent. Chemical Engineering Research and Design, 122, 151–163.
- Bulgariu, L., Lupea, M., Bulgariu, D., Rusu, C., & Macoveanu, M. (2013). Equilibrium study of Pb (II) and Cd (II) biosorption from aqueous solution on marine green algae biomass. Environmental Engineering & Management Journal (EEMJ), 12(1).
- Chan, K. H., Wong, E. T., Idris, A., & Yusof, N. M. (2015). Modification of PES membrane by PEG-coated cobalt doped iron oxide for improved Cu (II) removal. Journal of Industrial and Engineering Chemistry, 27, 283-290.
- Chen, J., Feng, J., & Yan, W. (2016). Influence of metal oxides on the adsorption characteristics of PPy/metal oxides for Methylene Blue. Journal of colloid and interface science, 475, 26-35.
- Dubinin, M.M. and Radushkevich, L.V. (1947) Equation of the Characteristic Curve of Activated Charcoal. Proceedings of the Academy of Sciences of the USSR, Physical Chemistry Section, 55, 331-333
- Duman, O., Tunç, S., Polat, T. G., & Bozoğlan, B. K. (2016). Synthesis of magnetic oxidized multiwalled carbon nanotube–κ-carrageenan–$Fe_3O_4$ nanocomposite adsorbent and its application in cationic methylene blue dye adsorption. Carbohydrate Polymers, 147, 79–88.
- Freundlich, H. M. F. (1906). Over the adsorption in solutions. Journal of Physical Chemistry, 57, 385–471.
- Ghaedi, M., Hossainian, H., Montazerozohori, M., Shokrollahi, A., Shojaipour, F., Soylak, M., & Purkait, M. K. (2011). A novel acorn-based adsorbent for the removal of brilliant green. Desalination, 281, 226–233.
- Guy, N., Çakar, S., & Ozacar, M. (2016). Comparison of palladium/zinc oxide photocatalysts prepared by different palladium doping methods for Congo red degradation. Journal of Colloid and Interface Science, 466, 128–137. https://doi.org/10.1016/j.jcis.2015.12.009
- Hem Lata, Garg, V. K., & Gupta, R. K. (2008). Adsorptive removal of basic dye by chemically activated Parthenium biomass: Equilibrium and kinetic modeling. Desalination, 219(1–3), 250–261.
- Hu, J., Lo, I. M. C., & Chen, G. (2007). Comparative study of various magnetic nanoparticles for Cr(VI) removal. Separation and Purification Technology, 56(3), 249–256. https://doi.org/10.1016/j.
- Hu, L., Yuan, H., Zou, L., Chen, F., & Hu, X. (2015). Adsorption and visible-light-driven photocatalytic degradation of Rhodamine B in aqueous solutions by Ag@AgBr/SBA-15. Applied Surface Science, 335, 706–715.
- Jia, Z., Li, Z., Li, S., Li, Y., & Zhu, R. (2016). Adsorption performance and mechanism of methylene blue on chemically activated carbon spheres derived from hydrothermally prepared poly(vinyl alcohol) microspheres. Journal of Molecular Liquids, 220, 56–62.
- Joshi, S., Garg, V. K., Kataria, N., & Kadirvelu, K. (2019). Applications of $Fe_3O_4$@AC nanoparticles for dye removal from simulated wastewater. Chemosphere, 236, 124280.
- Kadirvelu, K., Karthika, C., Vennilamani, N., & Pattabhi, S. (2005). Activated carbon from industrial solid waste as an adsorbent for the removal of Rhodamine B from aqueous solution: Kinetic and equilibrium studies. Chemosphere, 60(8), 1009–1017.
- Kataria, N., & Garg, V. K. (2019). Application of EDTA-modified $Fe_3O_4$/sawdust carbon nanocomposites to ameliorate methylene blue and brilliant green dye-laden water. Environmental Research, 172, 43–54.
- Khamparia, S., & Jaspal, D. (2016). Investigation of adsorption of Rhodamine B onto a natural adsorbent, Argemone mexicana. Journal of Environmental Management, 183, 786–793.
- Lagergren, S. (1898). Zur theorie der sogenannten adsorption gelöster stoffe. Vetenskapsakademiens Handlingar, 24, 1–39.
- Liqiang, J., Yichun, Q., Baiqi, W., et al. (2006). Review of photoluminescence performance of nano-sized semiconductor materials and its relationships with photocatalytic activity. Solar Energy Materials and Solar Cells, 90(12), 1773–1787. https://doi.org/10.1016/j.solmat.2005.11.007
- Liu, H., Hu, Y., Zhang, Z., et al. (2015a). Synthesis of spherical Ag/ZnO heterostructural composites with excellent photocatalytic activity under visible light and UV irradiation. Applied Surface Science, 355, 644–652. https://doi.org/10.1016/j.apsusc.2015.07.012

- Liu, K., Li, H., Wang, Y., Gou, X., & Duan, Y. (2015b). Adsorption and removal of rhodamine B from aqueous solution by tannic acid functionalized graphene. Colloids and Surfaces A: Physicochemical and Engineering Aspects, 477, 35–41.
- Ma, J., Zhu, W., Tian, Y., & Wang, Z. (2016). Preparation of zinc oxide–starch nanocomposite and its application on coating. Nanoscale Research Letters, 11, 200. https://doi.org/10.1186/s11671-016-1404-y
- Mahlambi, M. M., Ngila, C. J., & Mamba, B. B. (2015). Recent developments in environmental photocatalytic degradation of organic pollutants: The case of titanium dioxide nanoparticles—A review. Journal of Nanomaterials, 2015, 790173. https://doi.org/10.1155/2015/790173Malik, A. (2004). Metal bioremediation through growing cells. *Environment International, 30*(2), 261–278. https://doi.org/10.1016/j.envint.2003.09.001
- Malkoc, E. and Nuhoglu, Y. (2007) Potential of Tea Factory Waste for Chromium(VI) Removal from Aqueous Solutions: Thermodynamic and Kinetic Studies. Separation and Purification Technology, 54, 291-298.
- Mallakpour, S., & Madani, M. (2012). Use of silane coupling agent for surface modification of zinc oxide as inorganic filler and preparation of poly(amide–imide)/zinc oxide nanocomposite containing phenylalanine moieties. Bulletin of Materials Science, 35(3), 333–339. https://doi.org/10.1007/s12034-012-0304-8
- McKay, G., & Ho, Y. S. (1999). Pseudo-second order model for sorption processes. Process Biochemistry, 34(5), 451–465.
- Mehmood, A., Murtaza, G., Bhatti, T. M., & Kausar, R. (2017). Phyto-mediated synthesis of silver nanoparticles from Melia azedarach L. leaf extract: Characterization and antibacterial activity. Arabian Journal of Chemistry, 10(2), S3048–S3053. https://doi.org/10.1016/j.arabjc.2013.11.046
- Mu, B., Tang, J., Zhang, L., & Wang, A. (2016). Preparation, characterization, and dye adsorption performance of a well-defined two-dimensional superparamagnetic clay/polyaniline/$Fe_3O_4$ nanocomposite. Applied Clay Science, 132, 7–16.
- Mubarak, N. M., Fo, Y. T., Al-Salim, H. S., Sahu, J. N., Abdullah, E. C., Nizamuddin, S., Jayakumar, N. S., & Ganesan, P. (2015). Removal of methylene blue and Orange G from wastewater using magnetic biochar. International Journal of Nanoscience, 14(1), 1–13.
- Nazir, M. A., Khan, N. A., Cheng, C., et al. (2020). Surface-induced growth of ZIF-67 at Co-layered double hydroxide: Removal of methylene blue and methyl orange from water. Applied Clay Science, 190, 105564. https://doi.org/10.1016/j.clay.2020.105564
- Nazir, M. A., Najam, T., Shahzad, K., et al. (2022a). Heterointerface engineering of water-stable ZIF-8@ZIF-67: Adsorption of Rhodamine B from water. Surfaces and Interfaces, 34, 102324. https://doi.org/10.1016/j.surfin.2022.102324
- Nazir, M. A., Nazam, T., Jabeen, S., et al. (2022b). Facile synthesis of trimetallic layered double hydroxides (NiZnAl-LDHs): Adsorption of Rhodamine B and methyl orange from water. Inorganic Chemistry Communications, 145, 110008. https://doi.org/10.1016/j.inoche.2022.110008
- Nourmoradi, H., Ghiasvand, A. R., & Noorimotlagh, Z. (2015). Removal of methylene blue and acid orange 7 from aqueous solutions by activated carbon coated with zinc oxide (ZnO) nanoparticles: equilibrium, kinetic, and thermodynamic study. Desalination and water treatment, 55(1), 252-262.
- Peng, L., Qin, P., Lei, M., Zeng, Q., Song, H., Yang, J., Shao, J., Liao, B., & Gu, J. (2012). Modifying $Fe_3O_4$ nanoparticles with humic acid for removal of Rhodamine B in water. Journal of Hazardous Materials, 209–210, 193–198.
- Periyasamy, A. P. (2025). A review of bioremediation of textile dye containing wastewater. Cleaner Water, 4, 100092.
- Rodrigues, J., Hatami, T., Rosa, J. M., et al. (2020). Photocatalytic degradation using ZnO for the treatment of RB19 and RB21 dyes in industrial effluents and mathematical modeling of the process. Chemical Engineering Research and Design, 153, 294–305. https://doi.org/10.1016/j.cherd.2019.10.021
- Rouhi, M., Lakouraj, M. M., Tashakkorian, H., & Hasantabar, V. (2019). Novel carbon-based bioactive nanocomposites of aniline/indole copolymer for removal of cationic dyes from aqueous solution: Kinetics and isotherms. New Journal of Chemistry, 43(6), 2400–2410.
- Ruszkiewicz, J. A., Pinkas, A., Ferrer, B., et al. (2017). Neurotoxic effect of active ingredients in sunscreen products: A contemporary review. Toxicology Reports, 4, 245–259. https://doi.org/10.1016/j.toxrep.2017.05.006
- Sahu, I. P. (2023). Photodegradation of Methylene blue and Rhodamine B using potato starch mediated zinc oxide nanoparticles and its calcium nanocomposites: Greener approach.
- Saini, J., Garg, V. K., & Gupta, R. K. (2018). Removal of methylene blue from aqueous solution by $Fe_3O_4$@Ag/$SiO_2$ nanospheres: Synthesis, characterization, and adsorption performance. Journal of Molecular Liquids, 250, 413–422.
- Saini, J., Garg, V. K., Gupta, R. K., & Kataria, N. (2017). Removal of Orange G and Rhodamine B dyes from aqueous system using hydrothermally synthesized zinc oxide loaded activated carbon (ZnO–AC). Journal of Environmental Chemical Engineering, 5(2), 884–892
- Sinha, T., & Ahmaruzzaman, M. (2015). High-value utilization of egg shell to synthesize silver and gold–silver core-shell nanoparticles and their application for the degradation of hazardous dyes from aqueous phase—A green approach. Journal of Colloid and Interface Science, 453, 115–131. https://doi.org/10.1016/j.jcis.2015.04.053
- Sinha, T., Ahmaruzzaman, M., & Bhattacharjee, A. (2014). A simple approach for the synthesis of silver nanoparticles and their application as a catalyst for the photodegradation of methyl violet 6B dye under solar irradiation. Journal of Environmental Chemical Engineering, 2(4), 2269–2279. https://doi.org/10.1016/j.jece.2014.10.001
- Tan, P., Sun, J., Hu, Y., Fang, Z., Bi, Q., Chen, Y., & Cheng, J. (2015). Adsorption of Cu2+, Cd2+ and Ni2+ from aqueous single metal solutions on graphene oxide membranes. Journal of hazardous materials, 297, 251-260.
- Taylor, A.A., Tsuji, J.S., Garry, M.R., McArdle, M.E., Goodfellow, W.L., Adams, W.J., Menzie, C.A., 2020. Critical review of exposure and effects: Implications for setting regulatory health criteria for ingested copper. Environ. Manage. 65, 131–159. http://dx.doi.org/10.1007/s00267-019-01234-y.Temkin, M. J., & Pyzhev, V. (1940). Recent modifications to Langmuir isotherms. Acta Physicochimica, 12, 217–222.
- Uddin, M. T., Islam, M. A., Mahmud, S., & Rukanuzzaman, M. (2009). Adsorptive removal of methylene blue by tea waste. Journal of Hazardous Materials, 164(1), 53–60.
- Ul-Haq, A. N., Nadhman, A., Ullah, I., et al. (2017). Synthesis approaches of zinc oxide nanoparticles: The dilemma of ecotoxicity. Journal of Nanomaterials, 2017, 8510342. https://doi.org/10.1155/2017/8510342
- Wan, D., Li, W., Wang, G., et al. (2015). Adsorption and heterogeneous degradation of Rhodamine B on the surface of magnetic bentonite material. Applied Surface Science, 349, 988–996. https://doi.org/10.1016/j.apsusc.2015.05.004

- Wan, D., Wang, G., Chen, W. L. K., & Hu, L. L. Q. (2015). Adsorption and heterogeneous degradation of Rhodamine B on the surface of magnetic bentonite material. Applied Surface Science, 349, 988–996.
- Wang, S., & Zhu, Z. H. (2006). Characterisation and environmental application of an Australian natural zeolite for basic dye removal from aqueous solution. Journal of Hazardous Materials, 136(3), 946–952. https://doi.org/10.1016/j.jhazmat.2006.01.038
- Wolski, R., Bazan-Woźniak, A., Nosal-Wiercińska, A., & Pietrzak, R. (2024). Methylene blue and Rhodamine B dyes' efficient removal using biocarbons developed from waste. Molecules, 29(4022)
- Wu, X. L., Shi, Y., Zhong, S., Lin, H., & Chen, J. R. (2016). Facile synthesis of $Fe_3O_4$–graphene@mesoporous $SiO_2$ nanocomposites for efficient removal of methylene blue. Applied Surface Science, 378, 80–86.
- Yazdanbakhsh, M., Tavakkoli, H., & Hosseini, S. M. (2011). Characterization and evaluation of catalytic efficiency of $La_{0.5}Ca_{0.5}NiO$ nanopowders in removal of reactive blue 5 from aqueous solution. Desalination, 281, 388–395.
- Yu, M. D. (2010). Trichloroethylene toxicity. Agency for Toxic Substances and Disease Registry Case Studies in Environmental Medicine (CSEM). Atlanta, GA: ATSDR. tsdr.cdc.gov/csem/trichloroethylene/